AIAA JOURNAL
Vol. 33, No. 11, November 1995

Behavior of Pressure and Heat Transfer in Sharp Fin-Induced Turbulent Interactions

P. E. Rodi* and D. S. Dolling†
University of Texas at Austin, Austin, Texas 78712

An experimental study has been performed of sharp fin-induced shock wave/turbulent boundary-layer interactions at Mach 5 under moderately cooled wall conditions. The experimental data include mean surface pressure and heat transfer rate distributions for fin angles of attack of 6, 8, 10, 12, 14, and 16 deg. Data were acquired in spanwise and conical coordinate systems to assess the behavior of the surface properties. Although the surface pressure distributions collapse in conical coordinates, the heat transfer distributions do not. Instead, the heat transfer was found to be nearly constant along rays from a virtual conical origin determined from the pressure distributions.

Nomenclature

C_f = skin friction coefficient
C_h = Stanton number
$C_{h_{IP}}$ = Stanton number at initial peak heating
$C_{h_{pk}}$ = Stanton number at peak heating
$C_{h_{ref}}$ = reference Stanton number
h_{aw} = adiabatic surface enthalpy
h_w = surface enthalpy
M_∞ = freestream Mach number
P = mean surface pressure
P_e = surface pressure at interaction edge
P_{pk} = peak surface pressure
P_{pl} = plateau surface pressure
Pr = Prandtl number
q = mean surface heat transfer rate
q_o = stagnation point heat transfer
Re_θ = Reynolds number based on θ
Re_∞ = freestream Reynolds number
r = radial distance from VCO
T_{aw} = adiabatic surface temperature
T_w = surface temperature
X = downstream distance from fin leading edge
Y = spanwise distance normal to X from fin leading edge
Y_s = spanwise distance from fin to inviscid shock wave trace
Z = vertical distance measured upward from test surface
α_{SG} = shock generator angle
β = conical angle measured in the plane of the test surface
β_0 = angle of the trace of the inviscid shock wave
β_{A1} = angle of primary attachment
β_{S1} = angle of primary separation
β_{S2} = angle of secondary separation
β_U = angle of upstream influence
δ = boundary-layer thickness
δ^* = boundary-layer displacement thickness
θ = boundary-layer momentum thickness
μ_e = viscosity at boundary-layer edge
Π = boundary-layer wake strength parameter
ρ_e = density at boundary-layer edge
ϕ = conical angle above the surface

Received June 21, 1994; revision received Jan. 16, 1995; accepted for publication Jan. 23, 1995.

*Graduate Student, Center for Aeromechanics Research; currently Resident Research Associate, National Research Council, NASA Langley Research Center, Hampton, VA 23681. Member AIAA.

†Professor, Center for Aeromechanics Research. Associate Fellow AIAA.

Introduction

THE development of flight vehicles traveling at supersonic and hypersonic Mach numbers has brought with it a wide range of difficult problems for the aerodynamicist. One problem of practical importance is the inviscid/viscous interaction between a shock wave and a turbulent boundary layer. Local surface heat transfer and pressure can be unexpectedly high, and the unsteady nature of such large-scale separated interactions raises structural fatigue concerns. To understand these phenomena better, many investigations have been undertaken. Initially, many investigators studied flows that are nominally two dimensional, such as those generated by impinging planar shocks, steps, or unswept compression ramps. A review of much of this early work is presented in Ref. 1. However, most problems of practical interest are three dimensional.

One geometry generating a complex three-dimensional flowfield is that of an unswept sharp fin at angle of attack, α_{SG}, creating an attached planar inviscid shock wave that interacts with an incoming turbulent boundary layer (Fig. 1). The resulting flowfield has been studied both experimentally and numerically. Reviews of much of the work through the 1980s, with a discussion of many of the outstanding issues, are presented in Refs. 2 and 3.

In most of the experimental studies, for all but the smallest fin angles, a quasiconical region of large-scale boundary-layer separation occurs beyond an inception region near the fin leading edge (Fig. 2). Within the separated region a streamwise vortex is formed and extends downstream. The separated flow attaches just ahead of the fin/surface corner. Features of the interaction footprint, such as upstream influence and separation line locations, deduced from surface tracer techniques[4,5] and the mean pressure distributions[5] collapse in conical coordinates from a virtual conical origin (VCO). The rays defining important features of the interaction footprint are also shown in Fig. 2.

Semiempirical expressions have been developed for scaling features such as length of the inception region,[6] angle of upstream influence line,[4] and pitot and yaw angle profiles[7] over ranges of Mach and Reynolds numbers. More recent investigations using various optical techniques[8–10] have yielded much information about the flowfield structure in the conical "cross plane." Figure 3 shows a schematic of one such flowfield based on these studies. It is clear that in separated interactions, the inviscid shock wave bifurcates into a lambda-shock pattern. The inviscid flowfield between the lambda-shock intersection and the boundary layer appears to contain a transonic (in the cross plane) jet impinging on the surface just ahead of the fin. This jet impingement is believed to be responsible for the high-local-surface pressure and heat transfer. Although many interaction features collapse in a conical coordinate system, the skin friction distribution[11] does not. Since the heat transfer and skin friction both result from viscous effects, it might be anticipated that the skin friction

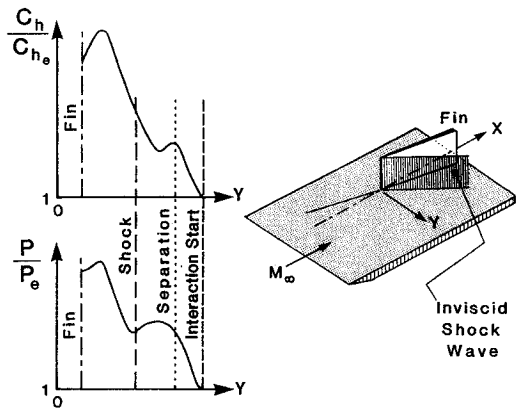

Fig. 1 Unswept sharp fin interaction, general features.

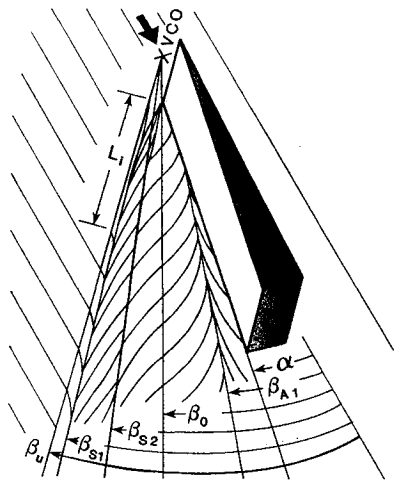

Fig. 2 Sketch of sharp fin interaction footprint.

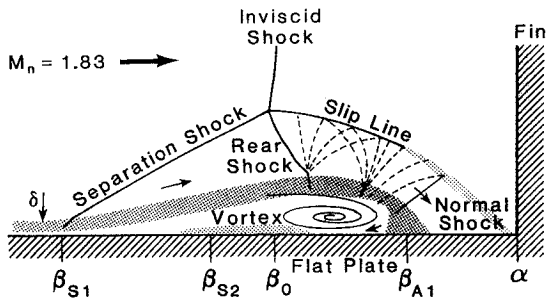

Fig. 3 Schematic from conical shadowgraph of crossflow plane, M_∞ = 3, α_{SG} = 20 deg interaction, from Alvi and Settles.[9]

distribution would provide some information on the character of the heat transfer distribution.

In a conical flowfield, the primary variables ρ, u, v, w, and T are described by the two conical angles, β and ϕ (i.e., constant along rays). However, quantities that involve derivatives of these variables (such as skin friction and heat transfer) are not necessarily constant along rays. For example, assume a ray is defined as (β_1, ϕ_1) where ϕ_1 is small (i.e., just above the surface). Along such a ray the temperature is constant, T_1. The surface temperature, T_w, is also constant and defined by the ray $(\beta_1, \phi = 0)$. By definition, the surface heat transfer is proportional to dT/dZ and is given by

$$q = -k\frac{dT}{dZ}$$

With increasing distance from the conical origin, the value of dT/dZ decreases. In fact, the temperature gradient dT/dZ is proportional to sin ϕ which, for small angles, equals $\Delta Z/r$ with r being the

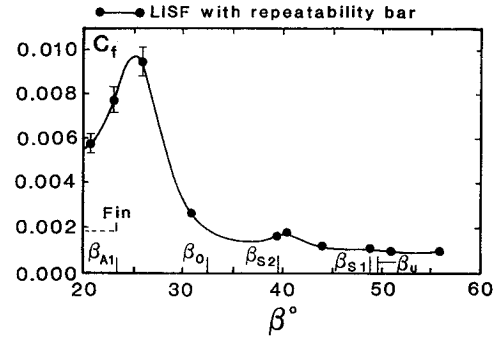

Fig. 4 Skin friction coefficient plotted against the conical angle β for M_∞ = 4, α_{SG} = 20 deg, based on Fig. 8 of Kim et al.[12]

radial distance from the conical origin. Therefore, $q = -kdT/dZ = -k\Delta Z/r$ or

$$qr = C_1 \qquad \text{and} \qquad C_h r = C_2$$

where C_1 and C_2 are constants. A similar behavior holds for the skin friction coefficient C_f.

The laser interferometer skin friction (LISF) technique has been used to study the skin friction distribution in these interactions.[11,12] The distribution in the conical cross plane exhibits small peaks located just outboard of the primary and secondary separation lines, as determined from surface flow visualization (SFV). Further inboard the skin friction increases to a peak value close to the fin. This peak can be an order of magnitude greater than the undisturbed level (Fig. 4). LISF data taken along rays from the VCO, determined from SFV, show a gradual increase in skin friction within the inception region and then a constant value beyond. This behavior is inconsistent with the conical flowfield model.

Many investigations of heat transfer in sharp fin-induced shock wave/turbulent boundary-layer interactions were made before the quasiconical nature of the interaction was understood. A typical spanwise heat transfer distribution across the interaction was shown in Fig. 1. The heat transfer rate rises above the undisturbed value and may have a local peak near the separation line. Further inboard, the heat transfer rapidly increases and reaches a peak value near the fin with a slight reduction in heating as the fin is reached. A number of semiempirical correlations have been developed for the magnitude[13] and location[14] of the peak heating value and for the magnitude[15] of the initial heating peak. These are discussed later in the paper. Recently, Lee et al.[16] measured the heat transfer in conical coordinates. Resistance temperature detector sensors were placed along two constant radius arcs measured from the fin leading edge. These data provide the heat transfer distribution in the conical cross plane. Using the normal Mach number, M_n, as an estimate of the interaction strength, an attempt was made to correlate the peak heat transfer q_{max}, by plotting q_{max} vs M_n. This was successful for interactions from Mach 3 to Mach 6. In their experiment, the radial distance between the arcs was small and no additional data were taken along conical rays to establish the behavior of the heat transfer distribution with radial distance from the conical origin. To the author's knowledge, no study has been conducted to investigate the heat transfer distribution along conical rays in sharp fin induced shock wave/turbulent boundary-layer interactions.

The purpose of the current research was, therefore, to determine the nature of the mean surface pressure and heat transfer distributions in such apparently conical interactions and determine whether the conical assumption is valid. This is an important question with many practical implications. For example, the use of such a simplifying assumption leads to greatly reduced computational requirements for computing these interactions, and it is important to understand the validity of this approach.

Experimental Program

Models and Flow Conditions

The experiments were performed in the 7 × 6 in. (17.8 × 15.2 cm) blowdown tunnel at the University of Texas at Austin. The tunnel

Table 1 Incoming boundary-layer properties

δ, in. (cm)	0.25 (0.64)
δ^*, in. (cm)	0.096 (0.24)
θ, in. (cm)	0.009 (0.023)
Re_θ	8340
C_f	0.00106
Π	0.72

uses air and was operated at a freestream Mach number, $M_\infty = 4.90$, total pressure of 315 psia +/− 3 psi (2.17 MPa) and total temperature of 760°R +/− 2°R (422 K). The nominal freestream Reynolds number was $Re_\infty = 11.6 \times 10^6$/ft ($38.1 \times 10^6$/m). Since the model was initially at ambient temperature, these test conditions produced a moderately cool wall with a model surface temperature to adiabatic surface temperature ratio, $T_w/T_{aw} = 0.8$.

The sharp fin model was made of stainless steel and was 6.00 in. (15.24 cm) long, 3.50 in. (8.89 cm) high, and 0.375 in. (0.95 cm) thick with a 11-deg bevel on the expansion side beginning at the leading edge. The fin was mounted normal to a brass flat plate with its leading edge 19.43 in. (49.35 cm) downstream of the plate leading edge. This location permitted natural transition of the boundary layer to occur well upstream of the interaction. With the fin removed, surveys of the pitot pressure through the boundary layer were made 0.5 in. (1.3 cm) upstream of the fin location. A pitot probe with an opening 0.050 in. (1.3 mm) spanwise by 0.014 in. (0.4 mm) high was used to obtain good spatial resolution within the boundary layer. The velocity profile was calculated from the pitot surveys. The static pressure measured at the wall (by a surface tap) was 15% greater than the freestream static pressure. To account for this variation, a linear static pressure distribution was assumed. Knowing the local static and pitot pressure, the Mach number could be determined using the Rayleigh pitot formula. An assumed total temperature distribution was used to convert the Mach number profile to a velocity profile. This temperature distribution was determined from a two-dimensional numerical solution of the boundary-layer equations. The actual total temperature is not expected to differ more than 9°R (5 K) from the assumed linear distribution over the region where the pitot data were acquired. A least-squares law-of-the-wall/law-of-the-wake curve fit was made of the velocity data using the approach of Sun and Childs.[17,18] The boundary-layer parameters determined from this fit are given in Table 1. Further details of the experiment are given in Ref. 19.

Pressure and Heat Transfer Measurements

Measurements included mean surface pressure and mean heat transfer distributions. The pressure measurements were made using pressure taps connected to a scanivalve. The scanivalve used a differential pressure transducer referenced to vacuum and calibrated using a Bourdon tube gauge, estimated to be accurate to within +/−0.02 psi. This uncertainty corresponds to about 3% of the freestream static pressure and 1% of the highest pressures within the interactions. Heat transfer rate was measured using commercially available Schmidt-Boelter gauges (Medtherm Corp., model #8-20-36-20903). These gauges contain a small substrate just under the measuring surface, such that heat transfer to the gauge creates a temperature gradient across the substrate which produces an output signal from a thermopile. The output voltage is then compared to a factory supplied calibration, and the heat transfer rate is determined. Each gauge is approximately 0.125 in. (3.2 mm) in diameter and also contains a T-type of thermocouple for the measurement of the surface temperature. The absolute accuracy of the heat transfer rate measurements is difficult to define precisely without an independent calibration. Therefore, the gauges were tested in two flows producing known heat transfer rates, and the results were used to determine the experimental uncertainty.

Heat transfer rate measurements were first made in the undisturbed flat plate turbulent boundary layer and compared to the Van Driest II (VDII) prediction[20] calculated from the known flow conditions. This case generates a heating rate at or below those in the sharp fin interaction. The gauges indicated an undisturbed heat transfer rate 10% below that predicted from the VDII method. However, the

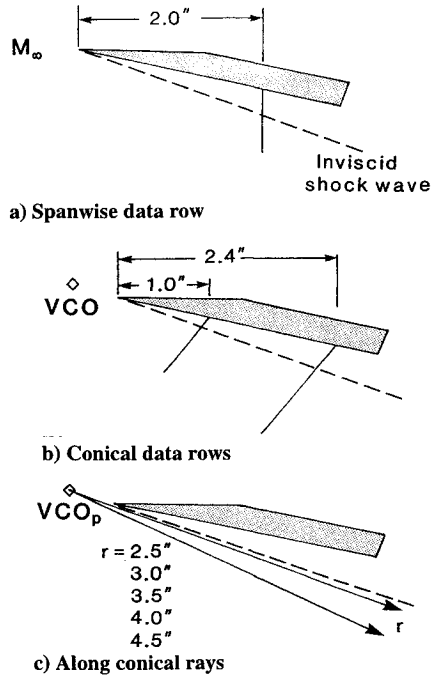

Fig. 5 Locations and orientations of transducer rows.

repeatability of the gauges over many runs was within +/−8%. The average measured heat transfer rate ($C_h = 0.00060$) was combined with the local skin friction coefficient determined from the law-of-the-wall/law-of-the-wake velocity fits ($C_f = 0.00106$) to determine the measured Reynolds analogy factor ($2C_h/C_f = 1.13$). This value for the Reynolds analogy factor is well within the data scatter in the literature.[21]

As a second test, the stagnation point heating on a probe in the Mach 4.90 freestream flow was measured. This heating rate is higher than that expected in the fin induced interactions. One Schmidt-Boelter gauge was installed in a small probe that was made in the shape of a circular cylinder and pointed end-on to the flow. The measured heat transfer was compared to the stagnation point heat transfer predicted from a self-similar solution of the compressible boundary-layer equations using the Lees-Dorodnitsyn transformation. Using this transformation, the expression for the stagnation point heat transfer to an axisymmetric body is

$$q_0 = 0.763 Pr^{-0.6} (\rho_e \mu_e)^{0.5} \sqrt{\frac{du_e}{ds}} (h_{aw} - h_w)$$

Boison and Curtis[22] have measured directly the velocity gradient at the stagnation point, du_e/ds, on a number of blunt axisymmetric shapes in a Mach 4.76 flow, and their results were used in the preceding expression. The predicted and measured values were within 8% for every calibration run. Thus, based on these two calibration experiments, measurements of the heat transfer footprint of the SW/TBL interactions are estimated to have a maximum uncertainty of +/−8%.

A 5.25-in.- (13.34-cm) diam brass instrumentation plug, which lay flush with the test surface, was built for the Schmidt-Boelter gauges. A similar plug was used for the pressure measurements. The face of each plug was divided into four transducer fields. Each field contained a similar pattern of transducer locations (or pressure taps) slightly offset from its location in each of the other fields. By rotating the plug 90, 180, and 270 deg from the initial orientation, data from different runs could be combined to improve the measurement point density. Mean surface pressure and heat transfer data were obtained along a spanwise row for angles of attack of 8 and 16 deg (shown schematically in Fig. 5a). Data were also taken along conical cross-plane rows (Fig. 5b). These conical orientations were obtained by simply rotating the instrumentation plugs. A third plug was made to measure the heat transfer along rays from a VCO (Fig. 5c). These data were taken to further explore the conical nature of the interaction footprint.

Results and Discussion

Spanwise Surface Pressure Measurements

As mentioned earlier, to improve the data density, each surface pressure and heat transfer distribution is composed of the results from two and four wind-tunnel runs, respectively. The scatter that such a technique can produce has been minimized by normalizing the data by the undisturbed values corresponding to each run. Examination of the kerosene-lampblack surface tracer patterns confirm that all spanwise pressure and heat transfer measurements were made within the quasiconical region of the interaction footprint. The lengths of the leading-edge inception regions and the upstream influence angles for each fin angle of attack, as determined from the surface tracer patterns, match previously developed semiempirical correlations indicating that these flowfields have scales and orientations consistent with earlier work.[19]

The pressure distributions along a spanwise row normal to the freestream direction located 2.0 in. (5.1 cm) or 8δ downstream of the fin leading edge are plotted in Fig. 6. For each case, the data have been normalized by the undisturbed pressure measured along the same row outboard of the interaction. The abscissa is the spanwise distance from the fin normalized by the spanwise distance from the fin to the trace of the inviscid shock wave, Y_s. For each fin angle of attack greater than 6 deg, the data are displaced upwards one unit of the ordinate. As expected, increasing the angle of attack increases both the physical scale of the interaction as well as its severity. For the smallest angle, the pressure rises very gradually from the undisturbed value. A small plateau region in evident just outside of the inviscid shock wave followed by a gradual rise as the fin is approached. The plateau pressure is defined as the maximum value in the plateau region. For higher angles of attack which generate a pressure distribution with a distinct peak-trough-peak shape, the plateau pressure is defined as the magnitude of the first peak. The peak pressure, P_{pk}, for the 6-deg case is 1.69 P_∞, compared to the theoretical value of 1.99 P_∞ from the oblique shock solution. In interactions such as these, the maximum pressure and heat transfer occur very close to fin. Spatial resolution constraints prohibit well-resolved measurements of the highest pressures near the fin/test surface junction.

Scuderi[15] has correlated both the peak pressure and the plateau pressure in terms of the normal Mach number

$$P_{pk}/P_\infty = 1.167M_n^{2.2} - 0.167 \quad (1)$$

for the peak pressure, and

$$P_{pl}/P_\infty = 2.75M_n^{0.5} - 1.75 \quad (2)$$

for the plateau pressure. Figure 7 shows a plot of the maximum measured pressure as a function of normal Mach number. Equation (1) is shown by a solid line. The discrepancy between the correlation and the measured maximum pressure is as high as 20%. However, the spatial resolution limitations mentioned earlier and believed to be the cause. The plateau pressures are also plotted in Fig. 7 as in Eq. (2). Once again there exists a discrepancy between the correlation and the current measurements, although to a lesser extent than with the peak pressure. This discrepancy cannot be attributed to spatial resolution, since the plateau region typically has a significant spatial extent.

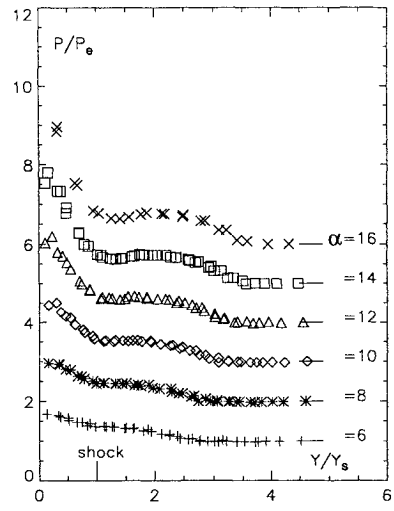

Fig. 6 Spanwise pressure distributions, M_∞ = 4.90.

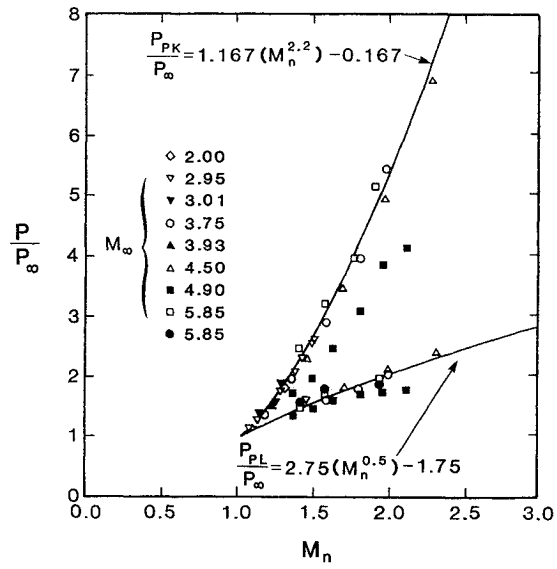

Fig. 7 Comparison of measured pressure peaks and Eqs. (1) and (2), from Scuderi.[15]

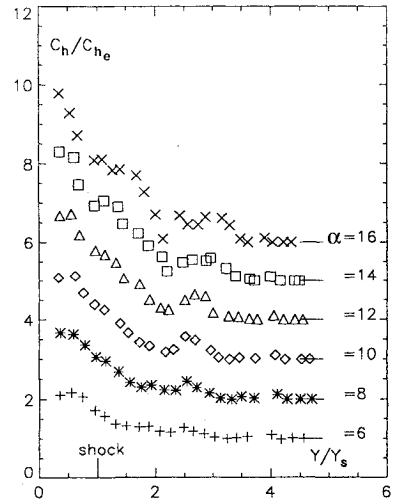

Fig. 8 Spanwise heat transfer distributions, M_∞ = 4.90.

Spanwise Heat Transfer Measurements

Heat transfer distributions along a spanwise row located 2.1 in. (5.1 cm) or 8δ downstream of the fin leading edge for each fin angle of attack are plotted in Fig. 8. The data are normalized by the undisturbed value at the interaction edge measured during each run. The length scale has again been normalized by the spanwise distance between the fin and the inviscid shock wave at this streamwise location. Again, for $\alpha_{SG} > 6$ deg the data are displaced upwards one unit of the ordinate.

As seen in the pressure results, increasing the angle of attack increases both the physical scale of the interaction as well as its severity. At each fin angle, the heat transfer rate begins increasing at essentially the same location as the pressure. Beginning at α_{SG} = 8 deg, a small peak in the heat transfer is seen just inboard of the start of the interaction. This peak grows in magnitude as the angle of attack is increased, reaching a value $C_{h_{IP}}/C_{h_e} = 1.7$ for α_{SG} = 16 deg. A similar peak was seen at α_{SG} = 10 deg at M_∞ = 3.95 in the study by Aso et al.[23] The normal Mach number is around 1.50 in

both cases. The heat transfer peak is much smaller in physical extent than that of the pressure plateau. Inboard of the first peak, the heat transfer rate drops to nearly undisturbed values creating a trough in the distribution. It then increases rapidly as the fin is approached.

As the fin angle is increased, the first peak and the trough in the heat transfer distribution move slightly outboard as the overall interaction grows. The width of the peak in normalized coordinates increases gradually with angle of attack although never reaching the extent of the pressure plateau. Within the region of rapid increase from the trough value to the maximum value, a slight inflection in the distribution develops for the two largest angles. The inflection point is located near the location of the trace of the inviscid shock wave. Similar features can be seen at $\alpha_{SG} = 10$ and 16 deg in the work of Aso et al.[23] at $M_\infty = 3.95$. Although the normal Mach number of the former case matches the present $\alpha_{SG} = 8$-deg case, no such inflection was seen in the current data. The normal Mach number of the latter case falls just above that of the current case of $\alpha_{SG} = 14$-deg. This inflection was not seen by Law[24] at Mach 6. However, the relatively poor spatial resolution of that study may be responsible for its absence.

The peak in the measured heat transfer distributions occurs very close to the fin, $Y/Y_s < 0.5$. Spatial resolution limits prevent locating the peak exactly. For each angle, the heat transfer peaks lie very close to the locations of the maximum measured pressure. Therefore, a single flowfield phenomenon may be responsible for both the peak in surface pressure and the peak in heat transfer.

Before the conical behavior of these types of flowfields was understood, Hayes[13] developed an empirical correlation for the peak heat transfer in the form

$$C_{h_{pk}}/C_{h_{ref}} = (M_\infty \sin\beta_0 - 1.0)n_{st} + 0.75 \qquad (3)$$

based on results up to $M_\infty = 5.85$ and $\alpha_{SG} = 20$ deg. The constant n_{st} is found from Fig. 9 and for the current position, $x/\delta = 8$, was set to 4.0. Recently, Lee et al.[16] and Settles[25] used the normal Mach number as a first-order measure of interaction strength and reported that the peak heating could be correlated by the following expression:

$$C_{h_{pk}}/C_{h_{ref}} = 3.7M_n - 2.7 \qquad (4)$$

for data in the range $3 < M_\infty < 6$. The current data are plotted with Eqs. (3) and (4) in Fig. 10. The agreement between the experimental data and these correlations is quite good.

Scuderi[15] used an expression based on two-dimensional pressure interaction theory to relate the normalized heating in the initial peak region to the normalized plateau pressure

$$C_{h_{IP}}/C_{h_{ref}} = (P_{pl}/P_\infty)^{0.85} \qquad (5)$$

The comparison between Eq. (5) and the current data is also shown in Fig. 10. Note, only data from cases with a clearly defined pressure plateau are plotted.

Overall, the agreement between the spanwise pressure and heat transfer distributions and correlations developed earlier is quite good. With the spanwise measurements indicating no unexpected flowfield phenomena, further examination of the interaction footprints could be made with confidence.

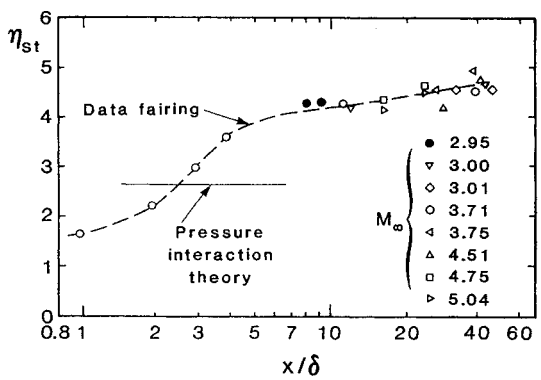

Fig. 9 Coefficient n_{st}, for Eq. (3), from Hayes.[13]

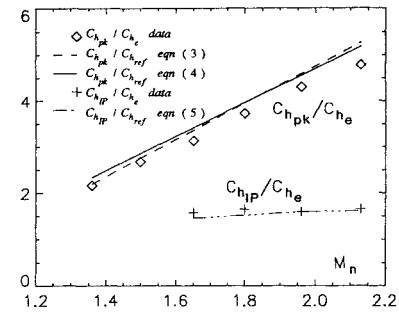

Fig. 10 Comparison of experimental heat transfer peaks to empirical correlations.

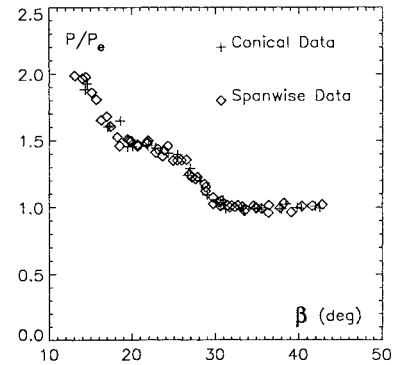

Fig. 11 Surface pressure in conical coordinates, $\alpha_{SG} = 8$ deg.

Conical Cross-Plane Measurements

To assess the conical behavior of the heat transfer and pressure distributions, additional measurements in the conical region were made with the instrumentation plugs rotated to align the rows of pressure taps and heat transfer gauges perpendicular to rays emanating from the VCO. Although it was not known a priori whether the pressure and heat transfer field would be conical, an initial assessment was possible by using a VCO determined from kerosene-lampblack surface flow visualization patterns (VCO_ν).[19] For the 8-deg case, the pressure plug was rotated clockwise 15 deg (as viewed from above) from the orientation used in the spanwise measurements. The two rows of pressure taps located at 0.92 in. (2.34 cm) and 2.35 in. (5.97 cm), or 3.7δ and 9.4δ, respectively, from the fin leading edge were used to acquire the data (see Fig. 5b). The value of 15 deg for the plug rotation was picked somewhat arbitrarily, being roughly half of β_U. This value of plug rotation permitted very close matching between the linear measurement rows and the curved conical cross planes of the interaction. For the 16-deg case, the instrumentation plugs were rotated clockwise 30 deg.

For both angles of attack, data measured along two rows in conical cross planes were analyzed, along with the spanwise data discussed earlier, in an attempt to locate a virtual conical origin based upon these pressure data (VCO_P). The technique used to locate the VCO_P consisted of four steps: 1) plotting the data against Y/Y_s, 2) identifying specific features (e.g., initial pressure rise, plateau, trough) and their locations in each distribution, 3) passing a straight line through the locations of the same feature on different distributions, and 4) determining the intersection of these pairs of lines. A number of different feature combinations were used to find the best overall choice of VCO_P for each angle. For these two fin angles, the pressure data were found to collapse in a conical reference frame (Figs. 11 and 12). The collapse of both the spanwise and conical pressure data is quite good, indicating the success in finding the VCO_P and the validity of the conical assumption when examining the pressure footprint. These VCO_P positions are located upstream of the fin leading edge and behind (away from the compression side of the fin) the extrapolated trace of the inviscid shock wave for both fin angles. The VCO_P locations, with respect to the fin leading edge, are presented in Table 2.

The heat transfer distributions in the conical cross plane were measured in a similar manner as the pressure distributions and are

Table 2 VCO_P locations

Directional component	$\alpha_{SG} = 8$ deg	$\alpha_{SG} = 16$ deg
(Streamwise distance from VCOP to fin leading edge)/δ	3.55	1.90
(Spanwise distance from VCOP to fin leading edge)/δ	1.44	0.91

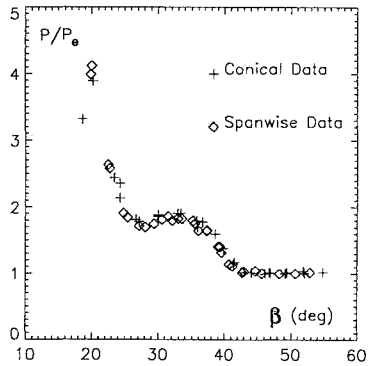

Fig. 12 Surface pressure in conical coordinates, α_{SG} = 16 deg.

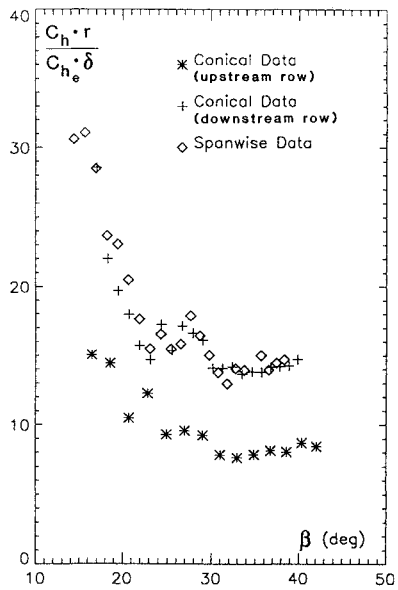

Fig. 13 Heat transfer in conical coordinates, α_{SG} = 8 deg.

plotted in Figs. 13 and 14 in $C_h r$ vs β coordinates from the VCOP. As mentioned earlier, in a conical flowfield the quantity $C_h r$ is a constant. In these two figures, the product $C_h r$ has been normalized by the quantity $C_{h_e}\delta$. The plots show both rows of conical heat transfer data along with the earlier spanwise heat transfer data. The heat transfer distributions do not collapse in a conical coordinate system using the VCOP as the origin, nor do they collapse if plotted using the VCO_v. This raised the question of whether a different VCO could be found to collapse the heat transfer data. As was done previously to locate the VCOP, key features of the heat transfer distributions were identified and used to locate a VCO based on the heat transfer distributions (VCO_h). However, no VCO_h could be found to collapse either set of heat transfer data.

In summary, the surface pressure measurements made along conical crossflow planes collapse very well using conical coordinates from a virtual conical origin, consistent with earlier experimental studies. However, no virtual conical origin could be found to collapse the heat transfer data in conical coordinates.

Measurements Along Conical Rays

To investigate the heat transfer distribution further, a third instrumentation plug was built in which heat transfer gauges were located along rays from the VCOP. This plug contained two rays,

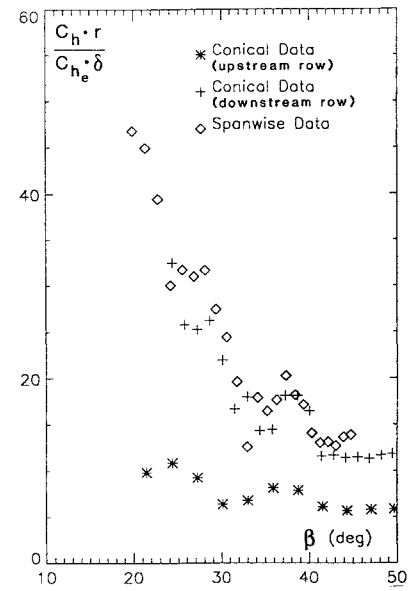

Fig. 14 Heat transfer in conical coordinates, α_{SG} = 16 deg.

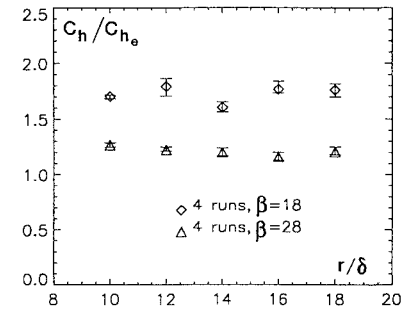

Fig. 15 Heat transfer along rays from VCOP, α_{SG} = 8 deg.

of five transducer ports each, positioned for $\alpha_{SG} = 8$ and 16 deg, as shown in Fig. 5c. Along each ray, transducers were placed at 2.50, 3.00, 3.50, 4.00, and 4.50 in. (6.36, 7.62, 8.89, 10.16, and 11.43 cm) from the VCOP. All of these stations are beyond the leading-edge inception region as determined from the surface tracer patterns.[19] Although the gauge positions were designed for a 16-deg. fin angle, tunnel starting difficulties limited the angle to 15 deg. This difference is not expected to have a significant impact on the results to be discussed. The reduced number of transducers employed permitted measurement of all of the gauges during the same wind-tunnel run, thereby avoiding the scatter which may occur when combining data from different runs.

The angles of the two rows of transducers were selected to match features of the conical pressure distributions. For the 8 deg case, the angles used for the transducer rows were $\beta = 18$ and 28 deg. The first angle corresponds to the kink in the pressure distribution between the plateau and the sharp rise near the fin (see Fig. 11). This position is just outside of the inviscid shock wave. The second angle was selected to fall within the initial pressure rise and to place the transducers along a ray whose angle is significantly different from the first. For the 16 deg case, the angles used for the transducer rows were $\beta = 27$ and 33 deg. The first angle corresponds to the trough between the pressure peak and the final pressure rise as seen in the distribution in Fig. 12. This ray is just outside of the inviscid shock wave. The second angle was selected to match the initial pressure peak of the pressure distribution.

The heat transfer measurements along conical rays from the each VCOP are shown in Figs. 15 and 16 for fin angles of 8 and 15 deg, respectively. The heat transfer has been normalized by the value of the undisturbed turbulent boundary-layer heat transfer measured by each gauge. Each data point is an average for all runs and is plotted along with its repeatability bar. Along both rays for each fin angle, the heat transfer is roughly constant. This behavior is

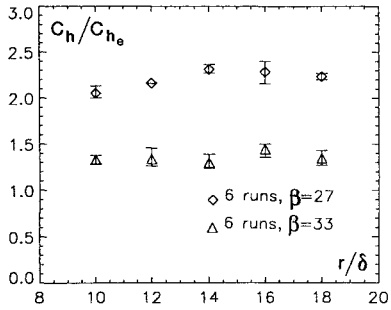

Fig. 16 Heat transfer along rays from VCO_P, α_{SG} = 15 deg.

very similar to that seen in the skin friction distributions by other investigators.[11] As seen earlier with the conical cross-plane data, no $1/r$ type behavior is seen, as would be expected with a purely conical flowfield.

Conclusions

Experimental measurements of mean surface pressure and heat transfer have been obtained for fin angles of attack from 6 to 16 deg at Mach 5. These data compare favorably with predictions from empirical correlations developed in earlier studies. Additional measurements have been made to study the behavior of the heat transfer distribution, specifically to examine whether or not it behaves quasiconically. The conclusions from this research are as follows:

1) Correlations based upon normal Mach number prove adequate for predicting the peak pressure, plateau pressure, and peak heating.

2) The mean surface pressure distributions display conical symmetry. A virtual conical origin of the pressure field was found for each case, and the pressure distributions collapse well when plotted in a conical coordinate system.

3) The mean surface heat transfer distributions are not conical. Heat transfer data, taken at 8- and 15-deg fin angle of attack, along rays from the virtual conical origin of the surface pressure field do not decay as would be expected in a purely conical flowfield, but instead are nearly constant.

Acknowledgments

The first author was supported by the NASA Graduate Researcher's Fellowship Program under NASA Training Grant NGT-50172. Additional support has been received from NASA, AFOSR, and the Office of Naval Research through the University of Texas at Austin's Center for Hypersonic Training and Research and from the Experimental Fluid Dynamics Branch of NASA Ames through San Jose State University/NASA Ames Research and Development Program. All of these sources of support are gratefully acknowledged as are the many useful discussions with C. C. Horstman of NASA Ames, D. D. Knight of Rutgers University, and G. S. Settles of Pennsylvania State University.

References

[1]Hankey, W. L., and Holden, M. J., "Two Dimensional Shock Wave Boundary Layer Interactions in High Speed Flow," AGARDograph 203, June 1975.

[2]Settles, G. S., and Dolling, D. S., "Swept Shock Wave/Boundary Layer Interactions," *Tactical Missile Aerodynamics*, edited by M. Hemsch, Progress in Astronautics and Aeronautics, AIAA, New York, 1992.

[3]Settles, G. S., and Dolling, D. S., "Swept Shock/Boundary-Layer Interactions—Tutorial and Update," AIAA Paper 90-0375, Jan. 1990.

[4]Lu, F. K., Settles, G. S., and Horstman, C. C., "Mach Number Effects on Conical Surface Features of Swept Shock Boundary-Layer Interactions," *AIAA Journal*, Vol. 28, No. 1, 1990, pp. 91–97.

[5]Lu, F. K., and Settles, G. S., "Conical Similarity of Shock/Boundary Layer Interactions Generated by Swept Fins," *AIAA Journal*, Vol. 23, No. 7, 1985, pp. 1021–1027.

[6]Lu, F. K., and Settles, G. S., "Inception Length to a Fully-Developed Fin-Generated Shock Wave Boundary-Layer Interaction," *AIAA Journal*, Vol. 29, No. 5, 1991, pp. 758–762.

[7]McClure, W. B., and Dolling, D. S., "Flowfield Scaling in Sharp Fin-Induced Shock Wave Turbulent Boundary Layer Interaction," *AIAA Journal*, Vol. 23, No. 2, 1985, pp. 201–206.

[8]Lu, F. K., and Settles, G. S., "Structure of Fin-Shock/Boundary-Layer Interactions by Laser Light-Screen Visualization," AIAA Paper 88-3801, July 1988.

[9]Alvi, F. S., and Settles, G. S., "Structure of Swept Shock Wave/Boundary-Layer Interactions Using Conical Shadowgraphy," AIAA Paper 90-1644, June 1990.

[10]Alvi, F. S., and Settles, G. S., "Physical Model of the Swept Shock Wave/Boundary-Layer Interaction Flowfield," *AIAA Journal*, Vol. 30, No. 9, 1992, pp. 2252–2258.

[11]Kim, K.-S., and Settles, G. S., "Skin Friction Measurements by Laser Interferometry in Swept Shock Wave/Turbulent Boundary-Layer Interactions," *AIAA Journal*, Vol. 28, No. 1, 1990, pp. 133–139.

[12]Kim, K.-S., Lee, Y., Alvi, F. S., Settles, G. S., and Horstman, C. C., "Skin Friction Measurements and Computational Comparison of Swept Shock/Boundary-Layer Interactions," *AIAA Journal*, Vol. 29, No. 10, 1991, pp. 1643–1650.

[13]Hayes, J. R., "Prediction Techniques for the Characteristics of Fin Generated Three Dimensional Shock Wave Turbulent Boundary Layer Interactions," AFFDL-TR-77-10, May 1977.

[14]Token, K. H., "Heat Transfer Due to Shock Wave Turbulent Boundary Layer Interactions on High Speed Weapon Systems," Air Force Flight Dynamics Lab., Dayton, OH, AFFDL-TR-74-77, April 1977.

[15]Scuderi, L. F., "Expression for Predicting 3-D Shock Wave-Turbulent Boundary Layer Interaction Pressures and Heating Rates," AIAA Paper 78-0162, Jan. 1978.

[16]Lee, Y., Settles, G. S., and Horstman, C. C., "Heat Transfer Measurements and Computations of Swept Shock Wave/Boundary-Layer Interactions," *AIAA Journal*, Vol. 32, No. 4, 1994, pp. 726–734.

[17]Sun, C.-C., and Childs, M. E., "A Modified Wall Wake Velocity Profile for Turbulent Compressible Boundary Layers," *Journal of Aircraft*, Vol. 10, No. 6, 1973, pp. 381–383.

[18]Sun, C.-C., and Childs, M. E., "Wall-Wake Velocity Profile for Compressible Nonadiabatic Flows," *AIAA Journal*, Vol. 14, No. 6, 1976, pp. 820–822.

[19]Rodi, P. E., "An Experimental/Computational Study of Heat Transfer in Sharp Fin Induced Shock Wave/Turbulent Boundary Layer Interactions at Low Hypersonic Mach Numbers," Ph.D. Dissertation, Dept. of Aerospace Engineering and Engineering Mechanics, Univ. of Texas at Austin, TX, Dec. 1991.

[20]Van Driest, E. R., "Turbulent Boundary Layer in Compressible Fluids," *Journal of the Aeronautical Sciences*, Vol. 18, No. 3, 1951, pp. 145–160, 216.

[21]Cary, A. M., "Summary of Available Information on Reynolds Analogy for Zero-Pressure-Gradient, Compressible, Turbulent-Boundary-Layer Flow," NASA TN D-5560, Jan. 1970.

[22]Boison, J. C., and Curtiss, H. A., "An Experimental Investigation of Blunt Body Stagnation Point Velocity Gradient," *ARS Journal*, No. 2, 1959, pp. 130–135.

[23]Aso, S., Tan, A., and Hayashi, M., "The Structure of Aerodynamic Heating in Three-Dimensional Shock Wave/Turbulent Boundary Layer Interactions Induced by Sharp and Blunt Fins," AIAA Paper 89-1854, June 1989.

[24]Law, C. H., "Three-Dimensional Shock Wave-Turbulent Boundary Layer Interactions at Mach 6," Aerospace Research Labs., ARL-TR-75-0191, Wright–Patterson AFB, OH, June 1975.

[25]Settles, G. S., private communication, June 1993.